JOURNAL OF THE AMERICAN CHEMICAL SOCIETY

Article

Tuning the Circumference of Six-Porphyrin Nanorings

Renee Haver, Lara Tejerina, Hua-Wei Jiang, Michel Rickhaus, Michael Jirasek, Isabell Gruebner, Hannah J. Eggimann, Laura M. Herz, and Harry L. Anderson

J. Am. Chem. Soc., **Just Accepted Manuscript** • Publication Date (Web): 24 Apr 2019

ACS Publications

is published by the American Chemical Society. 1155 Sixteenth Street N.W., Washington, DC 20036

Tuning the Circumference of Six-Porphyrin Nanorings

Renée Haver,†# Lara Tejerina,†# Hua-Wei Jiang,†# Michel Rickhaus,†# Michael Jirasek,# Isabell Grübner,# Hannah J. Eggimann,§ Laura M. Herz,§ and Harry L. Anderson*#

†These authors contributed equally.

#Department of Chemistry, University of Oxford, Chemistry Research Laboratory, Oxford OX1 3TA, United Kingdom

§Department of Physics, University of Oxford, Clarendon Laboratory, Parks Road, Oxford OX1 3PU, United Kingdom

ABSTRACT: Most macrocycles are made from a simple repeat unit, resulting in high symmetry. Breaking this symmetry allows fine tuning of the circumference, providing better control of the host-guest behavior and electronic structure. Here we present the template-directed synthesis of two unsymmetrical cyclic porphyrin hexamers with both ethyne (C2) and butadiyne (C4) links, and we compare these nanorings with the symmetrical analogues with six ethyne or six butadiyne links. Inserting two extra carbon atoms into the smaller nanoring causes a spectacular change in binding behavior: the template-affinity increases by a factor of 3 × 10^9, to a value of ca. 10^{38} M^{-1} and the mean effective molarity is ca. 830 M. In contrast, removing two carbon atoms from the largest nanoring results in almost no change in its template-affinity. The strain in these nanorings is 90–130 kJ mol^{-1}, as estimated both from DFT calculation of homodesmotic reactions and from comparing template-affinities of linear and cyclic oligomers. Breaking the symmetry has little effect on the absorption and fluorescence behavior of the nanorings: the low radiative rates that are characteristic of a circular delocalized S_1 excited state are preserved in the low-symmetry macrocycles.

Introduction

Symmetry confers beauty and simplicity. Most large synthetic macrocycles are constructed from a repeating monomer unit, resulting in a highly symmetric structure (C_n or D_{nh}), which expedites their synthesis and spectroscopic characterization, for example, it gives simple NMR spectra.[1] Conversely, a less symmetrical design brings structural versatility: it allows the diameter of the macrocycle to be adjusted in smaller increments, to optimize binding to a specific guest. In π-conjugated macrocycles, if the singlet electronic excited state is delocalized over the whole ring, high symmetry makes the S_0-S_1 transition forbidden; thus reducing the symmetry is expected to increase the radiative rate and increase the fluorescence quantum yield.[2,3] Previously, we reported the template-directed synthesis of two 6-fold symmetric cyclic porphyrin hexamers, ***c*-P6[b$_6$]** and ***c*-P6[e$_6$]**, linked *via* butadiyne (C4) and ethyne (C2) bridges, using templates **T6** and **T6***, respectively (Figure 1).[4-6] Here we show that low-symmetry (C_{2v}) versions of these macrocycles, ***c*-P6[b$_5$e]** and ***c*-P6[be$_5$]** can be synthesized using the same **T6** and **T6*** templates. We demonstrate that the ability to adjust the circumference, by adding or removing two carbon atoms, has a dramatic effect on the binding behavior of these nanorings. In contrast, the changes in symmetry are too subtle to have a strong effect on the radiative rates of the singlet excited states, and the photophysical behavior of the parent structures are preserved.

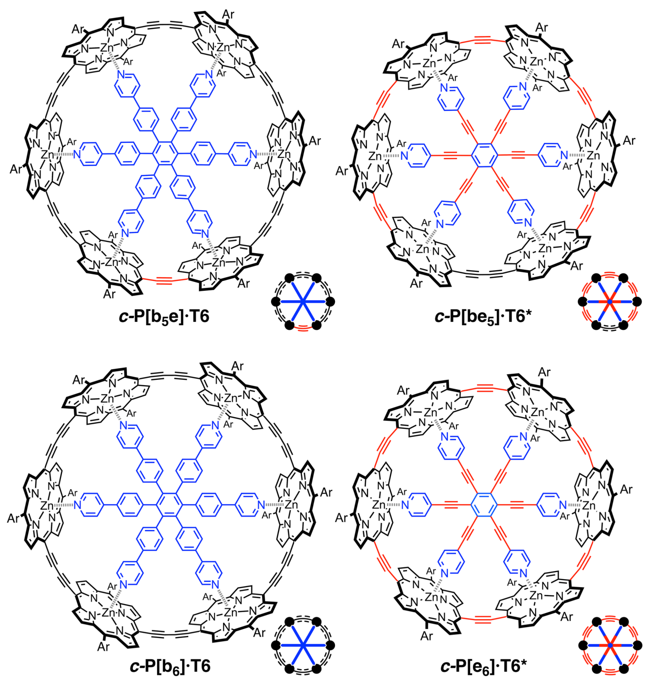

Figure 1. Molecular structures, schematic representation and labels of the porphyrin nanorings used throughout this study. The label in [brackets] indicates the number of butadiyne [b$_x$] or ethylene [e$_y$] linkages present in the nanoring. Ar = 3,5-bis(trihexylsilyl)phenyl.

Results and Discussion

Molecular Modeling. Density functional theory (DFT; B3LYP, 6-31G* basis set, in vacuum) was used to calculate optimized geometries of the free nanorings and their template complexes, to estimate the level of strain and to predict which templates would be effective for nanoring synthesis.[7] The strain in each nanoring (ΔH_{strain}) was estimated by calculating the free energy change for a homodesmotic reaction:[8] cyclic hexamer + linear dimer → linear octamer. The results (Table 1) show a gradual reduction in strain with ring expansion.

The complementarity of the templates was estimated from the average distances of the six zinc atoms from the centroid (R_{Zn}) for the template-free nanorings (Table 1). The ideal template radius ($R_{N,ideal}$) for each nanoring was calculated by subtracting the crystallographic out-of-plane distance of the zinc atom (0.37 Å) and the Zn-N(pyridine) bond length (2.15 Å) from R_{Zn}.[5] The calculated radii of **T6** and **T6*** (R_N) are 10.03 and 8.30 Å, respectively, allowing us to calculate the misfit ($R_N - R_{N,ideal}$) as listed in Table 1. These data lead to the surprising conclusion that, if we ignore the angular deviation from D_{6h} symmetry in the low-symmetry nanorings, then **T6*** and **T6** are expected to fit the unsymmetrical rings better than the symmetrical rings for which they were originally designed.[4,6] **T6** is slightly too small for ***c*-P6[b$_6$]** and slightly too big for ***c*-P6[b$_5$e]**, while **T6*** is slightly too big for ***c*-P6[be$_5$]** and substantially too big for ***c*-P6[e$_6$]**.

Table 1. Calculated Strains and Geometries from DFT.[a]

molecule	ΔH_{strain} (kJ mol^{-1})	R_{Zn} (Å)	$R_{N,ideal}$ (Å)	$R_N - R_{N,ideal}$ (Å)
***c*-P6[e$_6$]**	131	10.33	7.81	0.49 (**T6***)
***c*-P6[be$_5$]**	115	10.72	8.20	0.10 (**T6***)
***c*-P6[b$_5$e]**	105	12.38	9.86	0.17 (**T6**)
***c*-P6[b$_6$]**	100	12.82	10.30	–0.27 (**T6**)

[a] B3LYP/6-31G*; aryl groups replaced by H to facilitate calculations.

The DFT optimized geometries of the nanoring-template complexes (Figure 2) show that when the template is too large for the cavity, it adopts a domed conformation, rising above the plane of the nanoring, as seen clearly in ***c*-P6[e$_6$]·T6*** and to a more subtle extent in ***c*-P6[b$_5$e]·T6**.

Synthesis. The unsymmetrical nanorings were prepared from linear porphyrin hexamers, as summarized in Scheme 1. The key intermediate in the synthesis of ***c*-P6[b$_5$e]** is the C2-linked porphyrin dimer **TMS-*l*-P2[e]-CPDMS**, which was prepared by Sonogashira coupling of monomers **Br-P1-TMS** and **HC$_2$-P1-CPDMS**. This combination of silicon protecting groups with different polarities[9] was used to enable the C2-linked dimer to be separated from any C4-linked dimer by-product, **CPDMS-*l*-P2[b]-CPDMS**, produced by oxidative Glaser coupling of **HC$_2$-P1-CPDMS**. Traces of the butadiyne-linked byproduct must be removed, otherwise they lead to contamination of ***c*-P6[b$_5$e]** with symmetric ***c*-P6[b$_6$]**, which is inseparable. Complete deprotection of **TMS-*l*-P2[e]-CPDMS** followed by palladium-catalyzed oxidative coupling with excess **HC$_2$-P1-CPDMS** yielded porphyrin tetramer **CPDMS-*l*-P4[b$_2$e]-CPDMS** in 50% yield. This deprotection/coupling sequence was repeated to give porphyrin hexamer **CPDMS-*l*-P6[b$_4$e]-CPDMS** in good yield (68% over two steps). Deprotection of the hexamer followed by palladium-catalyzed oxidative coupling in the presence of **T6** template gave the target porphyrin nanoring ***c*-P6[b$_5$e]·T6** in 37% yield.

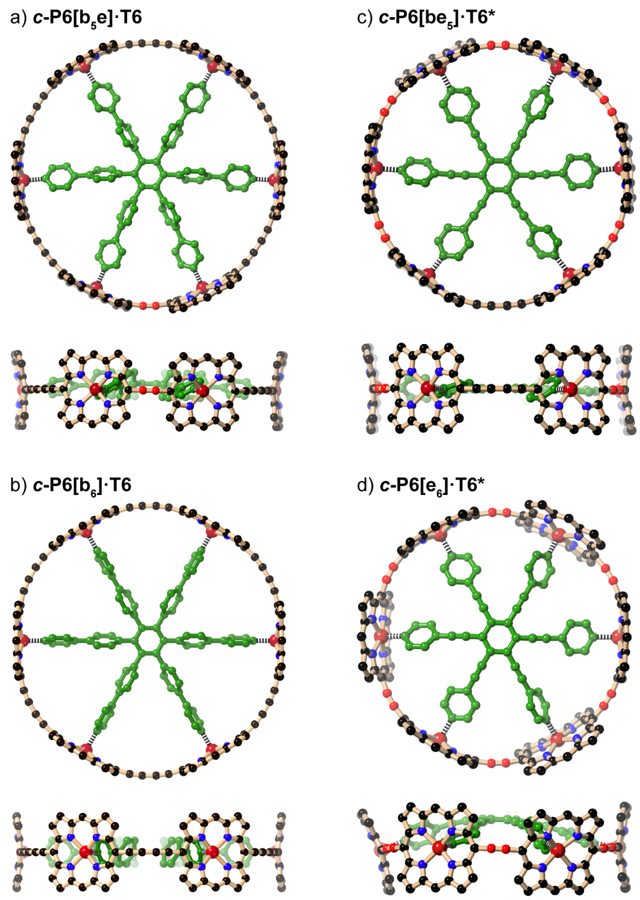

Figure 2. DFT calculated geometries of (a) ***c*-P6[b$_5$e]·T6**, (b) ***c*-P6[b$_6$]·T6**, (c) ***c*-P6[be$_5$]·T6***, and (d) ***c*-P6[e$_6$]·T6*** (two orthogonal views of each complex; B3LYP/6-31G*, aryl groups replaced by H to facilitate geometry optimization).

The smaller unsymmetrical nanoring ***c*-P6[be$_5$]·T6*** was synthesized in 25% yield, by palladium-catalyzed oxidative coupling of the linear C2-linked hexamer **HC$_2$-*l*-P6[e$_5$]-C$_2$H** in the presence of the **T6*** template. This linear hexamer was prepared from a known bromo-porphyrin hexamer[6] by Sonogashira coupling as shown in Scheme 1. The unsymmetrical nanoring ***c*-P6[be$_5$]** is easier to synthesize than ***c*-P6[e$_6$]**, both because oxidative Glaser coupling is a more efficient reaction than Sonogashira coupling, for the final cyclization step, and because the **T6*** template matches the cavity of ***c*-P6[be$_5$]** better than that of ***c*-P6[e$_6$]** (Table 1).

Scheme 1. Synthesis of *c*-P6[b$_5$e]·T6 and *c*-P6[be$_5$]·T6*

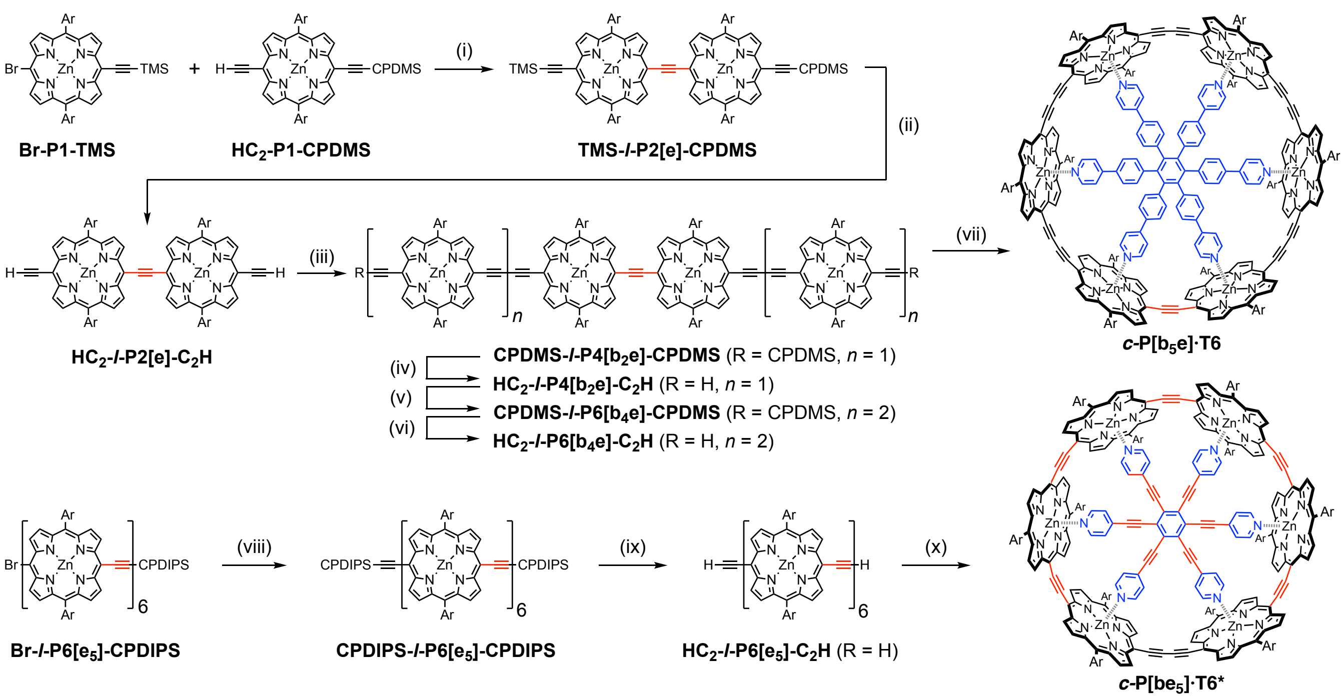

Reaction conditions: (i) $Pd_2(dba)_3$, $AsPh_3$, 64%. (ii) TBAF, 94%. (iii) **HC$_2$-P1-CPDMS**, $Pd(PPh_3)_2Cl_2$, CuI, 1,4-benzoquinone, 50%. (iv) TBAF, 100%. (v) **HC$_2$-P1-CPDMS**, $Pd(PPh_3)_2Cl_2$, CuI, 1,4-benzoquinone, 68%. (vi) TBAF, 100%. (vii) **T6**, $Pd(PPh_3)_2Cl_2$, CuI, 1,4-benzoquinone, 37%. (viii) CPDIPS-acetylene, $Pd(PPh_3)_2Cl_2$, CuI, 95%. (ix) TBAF, 96%. (x) **T6***, $Pd(PPh_3)_2Cl_2$, CuI, 1,4-benzoquinone, 25%. Ar = 3,5-bis(trihexylsilyl)phenyl. TMS = $SiMe_3$. CPDMS = $SiMe_2(CH_2)_3CN$. CPDIPS = $Si(i\text{-}Pr)_2(CH_2)_3CN$. The syntheses of the starting materials are detailed in the SI.

Table 2. Thermodynamic Parameters from UV-vis-NIR Titrations

porphyrin hexamer	ligand	log K_f	log $\overline{EM}$	ΔG_f (kJ mol^{-1})	ΔG_{strain} (kJ mol^{-1})
HC$_2$-*l*-P6[e$_5$]-C$_2$H	**T6***	15.8 ± 0.3	−1.6 ± 0.1	−90 ± 2	—
HC$_2$-*l*-P6[b$_4$e]-C$_2$H	**T6**	19.9 ± 0.3	−1.7 ± 0.1	−113 ± 2	—
HC$_2$-*l*-P6[b$_5$]-C$_2$H	**T6**	20.8 ± 0.3	−1.5 ± 0.1	−119 ± 2	—
***c*-P6[e$_6$]**	**T6***	29.0 ± 0.3	1.0 ± 0.1	−166 ± 2	76 ± 3 (*cf.* **HC$_2$-*l*-P6[e$_5$]-C$_2$H**)[a]
***c*-P6[be$_5$]**	**T6***	38.5 ± 0.3	2.9 ± 0.1	−220 ± 2	130 ± 3 (*cf.* **HC$_2$-*l*-P6[e$_5$]-C$_2$H**)
***c*-P6[b$_5$e]**	**T6**	35.6 ± 0.3	1.4 ± 0.1	−203 ± 2	90 ± 3 (*cf.* **HC$_2$-*l*-P6[b$_4$e]-C$_2$H**)
***c*-P6[b$_6$]**	**T6**	37.0 ± 0.3	1.7 ± 0.1	−211 ± 2	92 ± 3 (*cf.* **HC$_2$-*l*-P6[b$_5$]-C$_2$H**)

[a] The poor complementary between ***c*-P6[e$_6$]** and **T6*** mean that this value does not accurately reflect the strain in ***c*-P6[e$_6$]**.

NMR Spectroscopy. The ^{1}H NMR spectra of the four nanoring-template complexes are compared in Figure 3. Resonances from β-pyrrole protons nearest to an ethyne bridge are easy to identify by virtue of their high chemical shifts (*ca.* 10 ppm).[10] The spectra were fully assigned using 2D NMR techniques (as detailed in the SI). The complexes ***c*-P6[b$_6$]·T6** and ***c*-P6[e$_6$]·T6*** have D_{6h} symmetry on the NMR timescale, as reported previously,[4-6] whereas ***c*-P6[b$_5$e]·T6** and ***c*-P6[be$_5$]·T6*** have effective C_{2v} symmetry, resulting in splitting of the porphyrin and template resonances, as expected. The shielding of the α- and β-pyridine template protons is substantially greater in ***c*-P6[be$_5$]·T6*** than in ***c*-P6[e$_6$]·T6***, which probably reflects the tighter N-Zn interaction and less distorted geometry of ***c*-P6[be$_5$]·T6*** (Figure 2c,d).

Stabilities of Template Complexes: UV-vis-NIR and NMR Titrations. The stabilities of the nanoring-template complexes ***c*-P6[b$_6$]·T6**, ***c*-P6[b$_5$e]·T6**, ***c*-P6[be$_5$]·T6*** and ***c*-P6[e$_6$]·T6*** were determined by UV-vis-NIR titration, in toluene at 298 K, and compared with the corresponding complexes of linear porphyrin hexamers **HC$_2$-*l*-P6[b$_5$]-C$_2$H·T6**, **HC$_2$-*l*-P6[b$_4$e]-C$_2$H·T6** and **HC$_2$-*l*-P6[e$_5$]-C$_2$H·T6***. All the formation constants, K_f, are too high to be determined by direct titration, so they were measured by denaturation titrations, using a monovalent ligand to displace the template (pyridine or *N*-methylimidazole; for details, see SI).[4,11] Some examples of denaturation titration curves are plotted in Figure 4, showing that the stabilities of the nanoring complexes increase in the order ***c*-P6[e$_6$]·T6*** < ***c*-P6[b$_5$e]·T6** < ***c*-P6[b$_6$]·T6** <

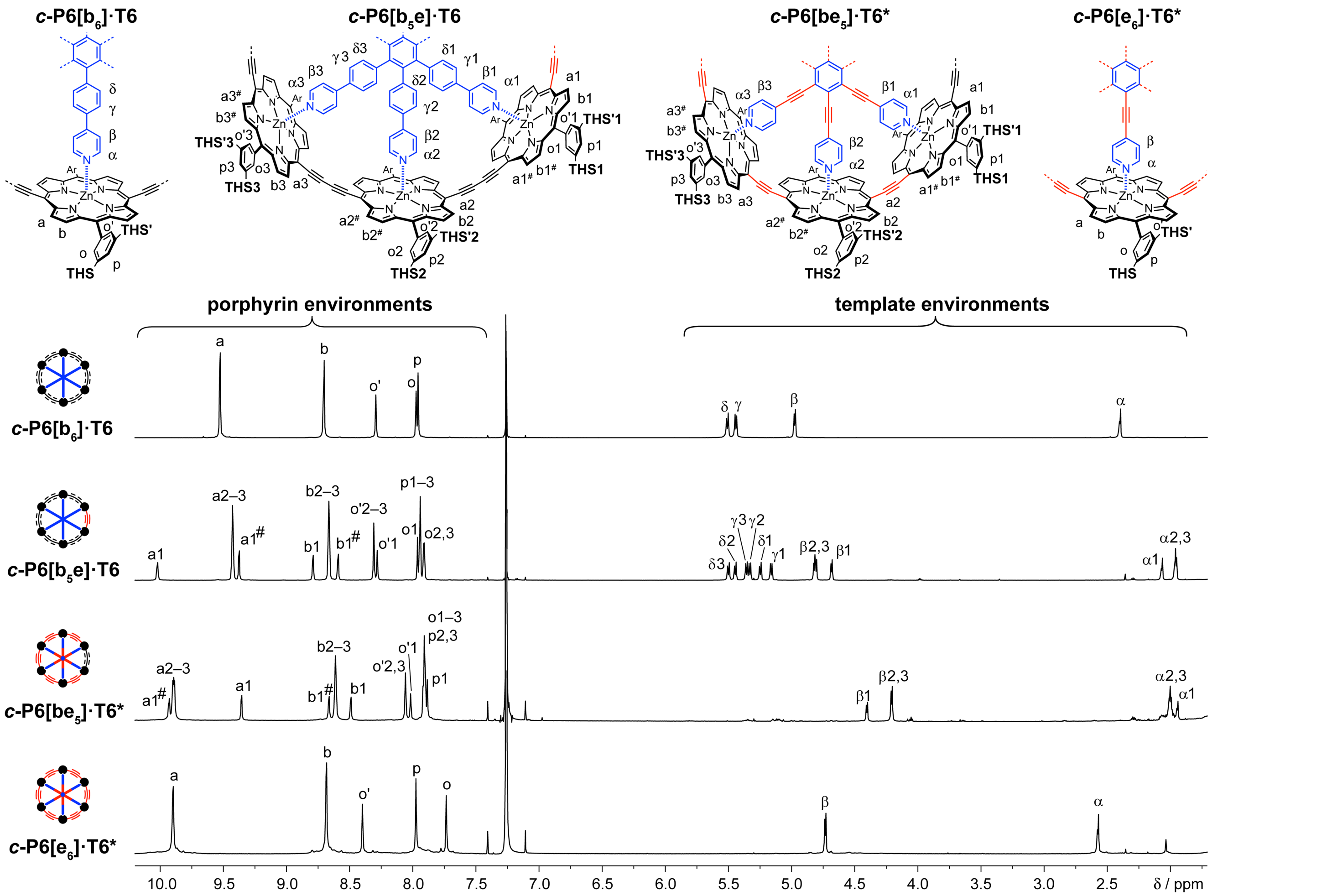

Figure 3. Partial ^{1}H NMR spectra of ***c*-P6[b$_6$]·T6**, ***c*-P6[b$_5$e]·T6**, ***c*-P6[be$_5$]·T6***, and ***c*-P6[e$_6$]·T6*** (700 MHz, $CDCl_3$, 298 K).

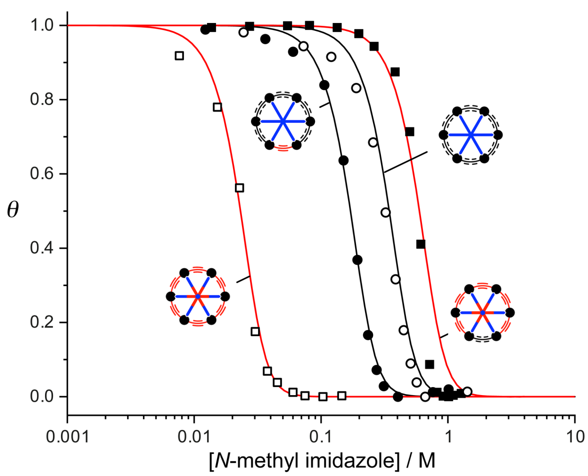

Figure 4. Denaturation curves for titration of ***c*-P6[b$_6$]·T6**, ***c*-P6[b$_5$e]·T6**, ***c*-P6[be$_5$]·T6***, and ***c*-P6[e$_6$]·T6*** with *N*-methyl imidazole. θ is the mole-fraction of nanoring bound to the template, estimated as $\theta = (A - A_f)/(A_i - A_f)$, where A, A_i and A_f are absorption, initial absorption and final absorption, respectively. Titrations were carried out in toluene at 298 K with a nanoring concentration of ca. 1 μM.

c*-P6[be$_5$]·T6. Nonlinear curve fitting of the titration data gave the values of logK_f listed in Table 2 (see SI for details). The nanorings all bind the templates much more strongly than the corresponding linear hexamers. Inserting two carbon atoms into ***c*-P6[e$_6$]** to give ***c*-P6[be$_5$]** results in a colossal increase in affinity for **T6***; logK_f increases from 29.0 to 38.5.

The level of chelate cooperativity[12,13] in the porphyrin hexamer template complexes was evaluated by calculating the effective molarities, $\overline{EM}$, by comparing the stability of each complex with that of a single-site reference interaction, using equation (1):

$$\overline{EM} = \sqrt[5]{\frac{K_{\mathrm{chem}}}{K_1^6}} \qquad (1)$$

where $\overline{EM}$ is the geometric mean of the effective molarities for five intramolecular interactions, K_{chem} is the statistically corrected formation constant of the hexamer-template complex ($K_{\mathrm{chem}} = K_f/768$) and K_1 is the statistically corrected binding constant of a monovalent reference ligand for a zinc porphyrin monomer. We use 4-phenylpyridine ($K_1 = 1.7 \times 10^4$ M^{-1}) as a reference for **T6** and 4-phenylethynylpyridine ($K_1 = 3.2 \times 10^3$ M^{-1}) as a reference for **T6***. The values of log$\overline{EM}$ listed in Table 2 highlight the exceptionally high chelate cooperativity of the ***c*-P6[be$_5$]·T6*** complex; log$\overline{EM}$ = 2.9 ± 0.1; $\overline{EM}$ = 830 ± 190 M. This is among the highest effective molarities found for any non-covalent supramolecular complex.[13-15]

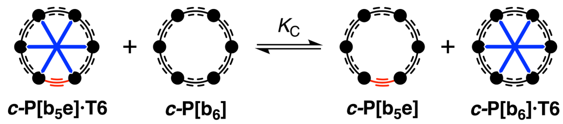

Figure 5. The position of this equilibrium was probed by [1]H NMR spectroscopy to measure the relative affinities of ***c*-P6[b$_6$]** and ***c*-P6[b$_5$e]** for **T6**.

The difference in formation constant between ***c*-P6[b$_6$]·T6** and ***c*-P6[b$_5$e]·T6** is surprisingly subtle. Presumably the weaker binding of ***c*-P6[b$_5$e]** reflect its lack of D_{6h} symmetry, because, according to our DFT calculations, its size-complementarity is better than that of ***c*-P6[b$_6$]** (Table 1). We carried out a [1]H NMR experiment to check the relative affinities of ***c*-P6[b$_6$]** and ***c*-P6[b$_5$e]** for **T6** in $CDCl_3$. The competition equilibrium constant K_C is defined as shown in Figure 5 and equation (2). The data from UV-vis-NIR denaturation titrations (Table 2) indicate that $\log K_C = 1.4 \pm 0.4$, in toluene at 298 K.

$$K_C = \frac{[c\text{-P6[b}_5\text{e]}][c\text{-P6[b}_6\text{]}\cdot\text{T6}]}{[c\text{-P6[b}_5\text{e]}\cdot\text{T6}][c\text{-P6[b}_6\text{]}]} = \frac{K_f(c\text{-P6[b}_6\text{]}\cdot\text{T6})}{K_f(c\text{-P6[b}_5\text{e]}\cdot\text{T6})} \qquad (2)$$

A 1:1 mixture of ***c*-P6[b$_6$]·T6** and ***c*-P6[b$_5$e]** was dissolved in $CDCl_3$ and *N*-methylimidazole was added to catalyze exchange of the template between the two nanorings. After equilibrium had been established, the ratio of ***c*-P6[b$_6$]·T6** to ***c*-P6[b$_5$e]·T6** was estimated by integration of the [1]H NMR spectrum (see SI for details). Within experimental error, the same mole ratio of complexes was formed by starting from a 1:1 mixture of ***c*-P6[b$_6$]** and ***c*-P6[b$_5$e]·T6**, confirming that this ratio reflects the position of thermodynamic equilibrium. At equilibrium, the [***c*-P6[b$_6$]·T6**]/[***c*-P6[b$_5$e]·T6**] ratio is 1.23 ± 0.10, giving $K_C = 1.5 \pm 0.2$ (in $CDCl_3$ at 298 K).

The strain energy in a porphyrin nanoring (ΔG_{strain}) can be estimated from the difference in binding energy of the template with the corresponding cyclic and linear oligomers, as expressed by equations (3).[4,16]

$$\Delta G_{strain} = \Delta G_f\,(\textbf{\textit{l}-P6}\cdot\text{template}) - \Delta G_f\,(\textbf{\textit{c}-P6}\cdot\text{template}) \qquad (3)$$

The values of ΔG_{strain} calculated in this way for ***c*-P6[be$_5$]**, ***c*-P6[b$_5$e]** and ***c*-P6[b$_6$]** (Table 2) are similar to the strain enthalpies from DFT (ΔH_{strain}, Table 1), indicating that the main cause for the weaker binding of the linear oligomers is the enthalpy cost of bending the linear oligomer into a cyclic conformation. This analysis assumes that there is no significant change in conformation, or increase in strain, when the nanoring binds the template, and that the strain in the bound linear oligomer is essentially the same as the strain in the nanoring. Equation (3) does not provide a good estimate of the strain if the template and/or nanoring undergo deformation on complexation, as is the case when ***c*-P6[e$_6$]** binds **T6***; here the low value of ΔG_{strain} reflects the poor shape complementarity between the nanoring and the template.

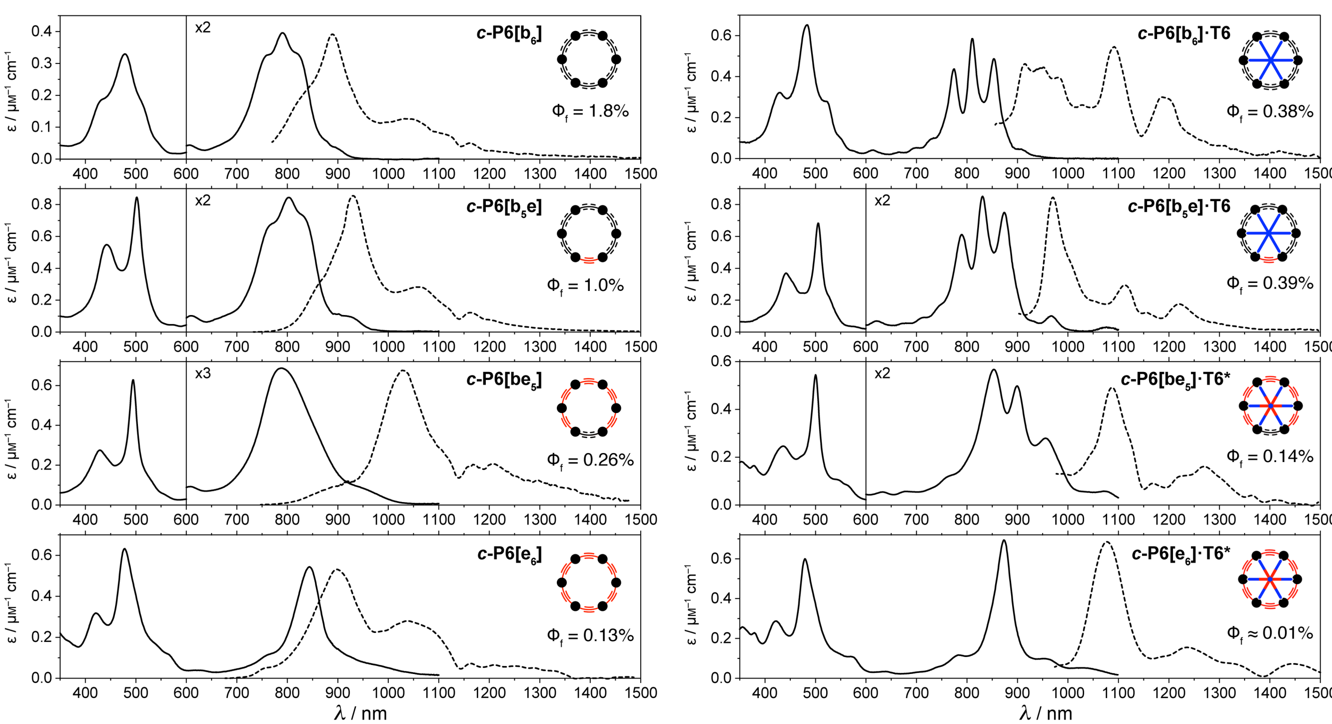

Figure 6. Absorption (black lines) and fluorescence (dashed lines) spectra at 298 K of (left) ***c*-P6[b$_6$]**, ***c*-P6[b$_5$e]**, ***c*-P6[be$_5$]**, ***c*-P6[e$_6$]** in toluene containing 1% pyridine and (right) ***c*-P6[b$_6$]·T6**, ***c*-P6[b$_5$e]·T6**, ***c*-P6[be$_5$]·T6***, ***c*-P6[e$_6$]·T6*** in toluene. Fluorescence quantum yields (Φ_f) are given in %. The dip in the fluorescence spectra at around 1140 nm is due to absorption by the solvent.

Table 3. Fluorescence lifetimes, quantum yields and radiative rates.[a]

compound	τ_f (ns)	Φ_f	k_{rad} (μs^{-1})
***c*-P6[e$_6$]**	0.49	0.0013	2.6
***c*-P6[be$_5$]**	0.28	0.0026	9.4
***c*-P6[b$_5$e]**	0.44	0.010	23
***c*-P6[b$_6$]**	0.51	0.018	35
c*-P6[be$_5$]·T6	0.22	0.0014	6.3
***c*-P6[b$_5$e]·T6**	0.32	0.0039	12
***c*-P6[b$_6$]·T6**	0.34	0.0038	11
THS-*l*-P6[b$_5$]-THS	1.43	0.28	400

[a] All measurements were carried out in toluene (containing 1% by volume of pyridine for the template-free nanorings to suppress aggregation). Fluorescence lifetimes were measured using excitation at 810 nm and detection at 1050 nm. Fluorescence quantum yields were measured using **THS-*l*-P6[b$_5$]-THS** as a standard.[17] Radiative rates are calculated as $k_{rad} = \Phi_f/\tau_f$.

Photophysical Behavior. The absorption and fluorescence spectra of the nanorings and their template complexes are compared in Figure 6. Fluorescence lifetimes, quantum yields and radiative rates are listed in Table 3.[17] The spectra of ***c*-P6[b$_6$]** and ***c*-P6[b$_5$e]** are very similar (with and without bound **T6**). There is more difference between the spectra of ***c*-P6[e$_6$]** and ***c*-P6[be$_5$]**, which probably reflects the greater strain in these complexes and the severe dome-shaped distortions in ***c*-P6[e$_6$]·T6*** (Figure 2d). Data for a typical linear hexamer, **THS-*l*-P6[b$_5$]-THS**, are also included in Table 3, for comparison. Linear conjugated porphyrin oligomers of this type generally have high radiative rates and fluorescence quantum yields.[17,18] All the nanorings have much lower fluorescence quantum yields and radiative rates than linear oligomers, as would be expected for a forbidden S_1-S_0 transition in a symmetrical circular π-system.[2,3,17] Comparison of the radiative rates for ***c*-P6[e$_6$]** and ***c*-P6[be$_5$]** suggests that in this case, lowering the symmetry increases the oscillator strength, but in general, the reduction in symmetry seems to be too subtle to have a strong effect on the photophysical behavior.

Conclusions

The template-directed synthesis of unsymmetrical porphyrin nanorings, with both ethyne (C2) and butadiyne (C4) links, opens up a new dimension in the investigation of conjugated porphyrin arrays.[10,19,20] Inserting two carbon atoms into the smallest nanoring, ***c*-P6[e$_6$]** causes a spectacular increase in its affinity for the template **T6***. The binding constant increases by a factor of 3×10^9, to a value of ca. 10^{38} M^{-1} and the mean effective molarity is ca. 830 M. Changing the size and symmetry has little effect on the absorption and fluorescence behavior of the nanorings. All the nanorings have much lower radiative rates than the corresponding linear oligomers, which implies that the S_1 excited state is delocalized around the circular π-system.

This work provides a dramatic demonstration of the importance of structural complementarity and preorganization in multivalent molecular recognition.[11,21] Nanoring-template binding constants can be tremendously sensitive to a geometrical mismatch, particularly if the template is too big for the cavity, as in ***c*-P6[e$_6$]·T6***. Even though **T6*** does not fit well in the cavity of ***c*-P6[e$_6$]**, it is still an effective template for directing the formation of this nanoring, probably because a template needs to be complementary to the transition state for cyclization, rather than complementary to the product.[7] This study also illustrates a new approach to estimating the strain in macrocyclic receptors, by comparing their guest-affinities with those of acyclic analogues. Strain free energies determined by this method (ΔG_{strain}, Table 2) agree remarkably well with strain enthalpies from DFT calculation of homodesmotic reactions (ΔH_{strain}, Table 1), in every case except that of the ***c*-P6[e$_6$]·T6*** complex where there is poor shape complementarity. This shows that the main barrier for bending a linear oligomer into a circular conformation is enthalpic rather than entropic.

ASSOCIATED CONTENT

Supporting Information. Synthetic procedures and characterization data; assignment of NMR spectra; UV-vis-NIR titrations; NMR competition experiments; photophysical characterization; computational chemistry and DFT calculations. This material is available free of charge via the Internet at http://pubs.acs.org

AUTHOR INFORMATION

Corresponding Author

harry.anderson@chem.ox.ac.uk

Funding Sources

No competing financial interests have been declared.

ACKNOWLEDGMENT

We thank the ERC (grant 320969), EPSRC (EP/M016110/1), the European Union's Horizon 2020 research and innovation programme (Marie Sklodowska-Curie grants MULTI-APP 642793 and SYNCHRONICS 643238) and the Swiss National Science Foundation (P2BSP2_168919) for funding, the EPSRC UK National Mass Spectrometry Facility at Swansea University for mass spectra and the University of Oxford Advanced Research Computing Service (ARC) for support. M.J. thanks Oxford University for a Scatcherd European Scholarship.

REFERENCES

(1) (a) Iyoda, M.; Yamakawa, J.; Rahman, M. J. Conjugated Macrocycles: Concepts and Applications. *Angew. Chem., Int. Ed.* **2011**, *50*, 10522–10533. (b) Grave, C.; Schlüter, A. D. Shape-Persistent, Nano-Sized Macrocycles. *Eur. J. Org. Chem.* **2002**, *2002*, 3075–3089. (c) May, R.; Jester, S.-S.; Höger, S. A Giant Molecular Spoked Wheel. *J. Am. Chem. Soc.* **2014**, *136*, 16732−16735. (d) Mayor, M.; Didschies, C. A Giant Conjugated Molecular Ring. *Angew. Chem. Int. Ed.* **2003**, *42*, 3176–3179.

(2) (a) Bednarz, M; Reineker, P.; Mena-Osteritz, E.; Bäuerle, P. Optical absorption spectra of linear and cyclic thiophenes—selection rules manifestation. *J. Lumin.* **2004**, *110*, 225–231. (b) Wong, B. M. Optoelectronic Properties of Carbon Nanorings: Excitonic Effects from Time-Dependent Density Functional Theory. *J. Phys. Chem. C* **2009**, *113*, 21921–21927. (c) Sundholm, D.; Taubert, S.; Pichierri, F. Calculation of Absorption and Emission Spectra of [*n*]Cycloparaphenylenes: the Reason for the Large Stokes Shift. *Phys. Chem. Chem. Phys.* **2010**, *12*, 2751–2757.

(3) (a) Parkinson, P.; Kondratuk, D. V.; Menelaou, C.; Gong, J. Q.; Anderson, H. L.; Herz, L. M. Chromophores in Molecular Nanorings: When Is a Ring a Ring? *J. Phys. Chem. Lett.* **2014**, *5*, 4356–4361. (b) J. Q. Gong, L. Favereau, H. L. Anderson, L. M. Herz, Breaking the Symmetry in Molecular Nanorings. *J. Phys. Chem. Lett.* **2016**, *7*, 332–338.

(4) Hoffmann, M.; Kärnbratt, J.; Chang, M.-H.; Herz, L. M.; Albinsson, B.; Anderson, H. L. Enhanced π-Conjugation around a Porphyrin[6] Nanoring. *Angew. Chem. Int. Ed.* **2008**, *47*, 4993–4996.

(5) Sprafke, J. K.; Kondratuk, D. V.; Wykes, M.; Thompson, A. L.; Hoffmann, M.; Drevinskas, R.; Chen, W.-H.; Yong, C. K.; Kärnbratt, J.; Bullock, J. E.; Malfois, M.; Wasielewski, M. R.; Albinsson, B.; Herz, L. M.; Zigmantas, D.; Beljonne, D.; Anderson, H. L. Belt-Shaped π-Systems: Relating Geometry to Electronic Structure in a Six-Porphyrin Nanoring. *J. Am. Chem. Soc.* **2011**, *133*, 17262–17273.

(6) Rickhaus, M.; Vargas Jentzsch, A.; Tejerina, L.; Grübner, I.; Jirasek, M.; Claridge, T. D. W.; Anderson, H. L. Single-Acetylene Linked Porphyrin Nanorings. *J. Am. Chem. Soc.* **2017**, *139*, 16502−16505.

(7) Bols, P. S.; Anderson, H. L. Template-Directed Synthesis of Molecular Nanorings and Cages. *Acc. Chem. Res.* **2018**, *51*, 2083−2092.

(8) Wheeler, S. E.; Houk, K. N.; Schleyer, P. v. R.; Allen, W. D. A Hierarchy of Homodesmotic Reactions for Thermochemistry. *J. Am. Chem. Soc.* **2009**, *131*, 2547–2560.

(9) Höger, S.; Bonrad, K. [(3-Cyanopropyl)dimethylsilyl]acetylene, a Polar Analogue of (Trimethylsilyl)acetylene: Synthesis and Applications in the Preparation of Monoprotected Bisacetylenes. *J. Org. Chem.* **2000**, *65*, 2243–2245.

(10) Lin, V. S.-Y.; DiMagno, S. G.; Therien, M. J. Highly Conjugated, Acetylenyl Bridged Porphyrins: New Models for Light-Harvesting Antenna Systems. *Science* **1994**, *264*, 1105–1111.

(11) Hogben, H. J.; Sprafke, J. K.; Hoffmann, M.; Pawlicki, M.; Anderson, H. L. Stepwise Effective Molarities in Porphyrin Oligomer Complexes: Preorganization Results in Exceptionally Strong Chelate Cooperativity. *J. Am. Chem. Soc.* **2011**, *133*, 20962–20969.

(12) Hunter, C. A.; Anderson, H. L. What is Cooperativity? *Angew. Chem. Int. Ed.* **2009**, *48*, 7488–7499.

(13) Motloch, P.; Hunter, C. A. Thermodynamic Effective Molarities for Supramolecular Complexes. *Adv. Phys. Org. Chem.* **2016**, *50*, 77–118.

(14) Montoro-García, C.; Camacho-García, J.; López-Pérez, A. M.; Bilbao, N.; Romero-Pérez, S.; Mayoral, M. J.; González-Rodríguez, D. High-Fidelity Noncovalent Synthesis of Hydrogen-Bonded Macrocyclic Assemblies. *Angew. Chem. Int. Ed.* **2015**, *54*, 6780–6784.

(15) Montoro-García, C.; Camacho-García, J.; López-Pérez, A. M.; Mayoral, M. J.; Bilbao, N.; González-Rodríguez, D. Role of the Symmetry of Multipoint Hydrogen Bonding on Chelate Cooperativity in Supramolecular Macrocyclization Processes. *Angew Chem. Int. Ed.* **2016**, *55*, 223–227.

(16) Hoffmann, M.; Wilson, C. J.; Odell, B.; Anderson, H. L. Template-Directed Synthesis of a π-Conjugated Porphyrin Nanoring. *Angew. Chem., Int. Ed.* **2007**, *46*, 3122–3125.

(17) Yong, C. K.; Parkinson, P.; Kondratuk, D. V.; Chen, W.-H.; Stannard, A.; Summerfield, A.; Sprafke, J. K.; O'Sullivan, M. C.; Beton, P. H.; Anderson, H. L.; Herz, L. M. Ultrafast delocalization of excitation in synthetic light-harvesting nanorings. *Chem. Sci.* **2015**, *6*, 181–189.

(18) Duncan, T. V.; Susumu, K.; Sinks, L. E.; Therien, M. J. Exceptional near-infrared fluorescence quantum yields and excited-state absorptivity of highly conjugated porphyrin arrays. *J. Am. Chem. Soc.* **2006**, *128*, 9000–9001.

(19) Tanaka, T.; Osuka, A. Conjugated Porphyrin Arrays: Synthesis, Properties and Applications for Functional materials. *Chem. Soc. Rev.* **2015**, *44*, 943–969.

(20) Holten, D.; Bocian, D. F.; Lindsey, J. S. Probing Electronic Communication in Covalently Linked Multiporphyrin Arrays. A Guide to the Rational Design of Molecular Photonic Devices. *Acc. Chem. Res.* **2002**, *35*, 57–69.

(21) (a) Cram, D. J. Preorganization from Solvents to Spherands. *Angew. Chem., Int. Ed. Engl.* **1986**, *25*, 1039–1057. (b) Sun, H.; Navarro, C.; Hunter, C. A. Influence of Non-Covalent Preorganization on Supramolecular Effective Molarities. *Org. Biomol. Chem.* **2015**, *13*, 4981–4992. (c) Martí-Centelles, V.; Pandey, M. D.; Burguete, M. I.; Luis, S. V. Macrocyclization Reactions: The Importance of Conformational, Configurational, and Template-Induced Preorganization. *Chem. Rev.* **2015**, *115*, 8736−8834.

TOC Figure